Self-Assembly of Ionically End-Capped Diblock Copolymers

Volker Schädler, Volker Kniese, Thomas Thurn-Albrecht, Ulrich Wiesner,* and Hans W. Spiess

Max-Planck-Institut für Polymerforschung, Postfach 3148, D-55021 Mainz, Germany

Received December 22, 1997; Revised Manuscript Received April 23, 1998

ABSTRACT: The self-assembly of ionically end-capped, symmetric polystyrene−polyisoprene diblock copolymers (PS-*b*-PI) has been studied. Structural data obtained from small-angle X-ray scattering (SAXS) and transmission electron microscopy (TEM) were correlated with the aggregation behavior of charged chain ends as evidenced by a spin probe using electron paramagnetic resonance (EPR) spectroscopy. The resulting mesomorphic structures were shown to be determined by the chain end topology, i.e., the site where the ionic chain end has been introduced chemically: For ω-functionalized diblock copolymers (monofunctional species) microphase separation is significantly stabilized due to the presence of ionic aggregates within the respective phase separated homopolymer domains. In contrast, for salt-free α,ω-macrozwitterionic diblock copolymers a marked perturbation of the block copolymer superstructure was found. In this case, the formation of a network of mixed ionic aggregates creates an additional microdomain interface by joining the chemically distinct blocks at their chain ends. The alteration of the degree of microphase separation as observed for the different functionalities can be attributed to conformational changes of the copolymer chain. Chain end association in the present system is reminiscent of certain covalently joined star and graft copolymers.

Introduction

Ordered phases on a mesoscopic scale play an important role in a wide range of fields from biology to materials science. As an example, the self-assembly of block copolymers has fascinated scientists for more than 3 decades[1,2] and can be considered in close analogy to the phase behavior of lyotropic liquid crystals (LC's), including lipids and surfactants.[3] Their supramolecular structure is largely dictated by the composition f, the overall degree of polymerization, N, and the effective segment−segment compatibility, expressed by Flory's parameter χ. While in the classical mean-field picture only f and χN determine the physical state,[4] fluctuation and conformation effects are now included to account for the complex phase behavior near the order−disorder transition (ODT).[5,6]

To further manipulate the morphology, several possibilities have been explored: On the basis of chlorosilane chemistry and the anionic polymerization technique, new block copolymer architectures were explored. Hadjichristidis et al. synthesized H- or π-shaped topologies[7,8] as well as different star-shaped polymers, containing identical or different arms.[9,10] Structure analysis reveals that for a given N and f, different equilibrium phases are accessible by varying chain topology.[11] A third component, as revealed by the studies on ABC triblock copolymers by Stadler and coworkers,[12] provides access to so far unknown structures such as the "ball at the wall" morphology[13] or phases which contain chiral mesoscopic elements.[14] The morphology can further be influenced by including additional interactions introducing, e.g., semicrystalline blocks[15] or mesogen-containing blocks.[16,17] The overall self-organizing behavior can then be described in terms of "tandem molecular interactions",[18] i.e., the interference of at least two distinct types of self-assembly processes. Striking morphologies have recently been observed for amorphous block copolymers which were functionalized with LC side groups[19,20] or consisted of the building blocks amorphous/LC main chain,[21,22] semicrystalline/LC side chain,[21,23] or LC side chain/LC main chain.[24]

Here we will show how morphology can be controlled by *ionic chain ends* and how this is related to their self-assembly. From ionically end-capped homopolymers it is well-known that charged end groups, in a medium of low dielectric constant, form aggregates often termed as multiplets.[25] They can be viewed as inverted micelles, where the core consists of nondissociated ion pairs.[26] Besides monofunctionalized diblock copolymers, we considered macromolecules bearing *oppositely* charged chain ends, i.e., α,ω-macrozwitterions. Up to recently, this had been a synthetical challenge, as reported for α,ω-macrozwitterionic homopolymers.[27,28] Such a telechelic system is different from the case of having a dipole at one chain end, since association of *unlike* chain ends, thus unlike blocks, has to occur.

Following the synthesis and characterization of α,ω-macrozwitterionic diblock copolymers of styrene and isoprene,[29] we have shown first results on the structure of mono- and bifunctionalized PS-*b*-PI's in the solid state.[30] The morphology of the end-capped species depends on whether only one or both chain ends are ionically end-functionalized. The impact of the ionic chain ends on the microphase separation can be gradually "switched off" by the addition of low molecular salt,[30] in analogy to the screening of coulomb interactions in polyelectrolytes. Fine tuning of morphological parameters as the lamellar spacing thus becomes possible.

To reveal the nature of the present "tandem molecular interactions", a detailed description of ionic aggregation is necessary. This is achieved in the present study by using EPR spectroscopy. This tool enables one to characterize the local dynamics of ion aggregates, which are largely governed by the nature of the ionic chain end as well as the nature of the polymer backbone.[31] By combining the EPR results with structural data as

* To whom correspondence should be addressed.

S0024-9297(97)01843-3 CCC: $15.00
Published on Web 06/27/1998

obtained by SAXS and TEM we will then give a full account of the self-assembly in the present model macromolecular systems.

Experimental Section

Materials and Sample Preparation. All end-capped block copolymers were synthesized by means of anionic polymerization using the procedure described in ref 29. The MW characteristics were obtained by size exclusion chromatography (SEC) using narrow calibration PS standards and ^{1}H NMR spectroscopy (Bruker AC 300).

For SAXS measurements, all samples were precipitated from THF into methanol, pressed into disks, and then annealed at 120 °C under vacuum for 20 h.

For spin probe studies, the potassium salt of 4-carboxy-TEMPO[32] was used, abbreviated K-TEMPO. It was obtained by neutralizing 4-carboxy-TEMPO (Aldrich) with 0.1 M methanolic KOH. All samples were prepared by the solvent casting method: 100 mg of the polymer dissolved in 10 mL of toluene were mixed with the calculated amount of a 0.05% methanolic spin probe solution such that the ratio of spin probes per ionic chain ends did not exceed $^1/_{15}$. After solvent evaporation, the samples were transferred into an EPR tube and annealed under vacuum at 120 °C for >6 h.

Dialysis. Salt-free α,ω-macrozwitterionic diblock copolymers were obtained by dialysis using membranes of regenerated cellulose (Spectra/Por MWCO:1000, Carl Roth GmbH & Co.) in a mixture of toluene/methanol (4/1). The counterion content was checked by neutron activation analysis at the Institut für Kernchemie, Johannes-Gutenberg Universität, Mainz.

DSC. Differential scanning calorimetry measurements (DSC) were carried out with a Mettler compensation calorimeter (DSC-30) using a heating/cooling rate of 10 K/min. Evaluation of the DSC curves was performed by using the software package from the same company.

TEM. Samples for TEM were obtained from annealed block copolymer disks: The OsO_4-stained polymers were cut into ultrathin sections and then exposed to OsO_4 for another 6 h. For electron microscopical observation a Zeiss EM 902 instrument was used. Micrographs were recorded on a Kodak FGPR 35 mm film.

SAXS. All measurements were performed with a Kratky compact camera (Anton Paar KG) equipped with a one-dimensional position-sensitive detector (M. Braun). The Ni-filtered Cu Kα radiation ($\lambda = 0.154$ nm) from a sealed X-ray tube was used. The samples were kept in the camera under vacuum in a special brass furnace (sample thickness 1 mm). Measuring time for all samples was 30 min. Smeared intensity data were corrected for absorption, background scattering, and slit-length smearing.[33] Intensities in absolute units were determined by using the moving slit method. Temperature-dependent measurements were performed with a relative stability better than 0.2 K, using a temperature controller. Changes between successive temperatures were completed within ca. 3 min, and a waiting time of 15 min was preset for equilibration.

EPR. Spectra were recorded on a Bruker ESP 300 instrument (X-band, ca. 9.45 GHz), equipped with a variable temperature accessory (ER 4111 VT). The modulation amplitude was set to 0.2 G by using a calibration with fluoranthrenylantimony hexafluoride. In this work the temperature-dependent extreme outer peak separation of the measured TEMPO spectrum is termed $2\tilde{A}_{zz}$, to avoid confusion with the tensor component in the rigid limit $2A_{zz}$, see below.[34]

Analysis of EPR Spectra. After basic data processing of all measured spectra (i.e., baseline correction with polynomials of third order, normalization with respect to the number of spins, and field axis alignment by shifting the data to the same spectral center), three adequately chosen EPR spectra of the respective model components (as described under Results, section 3) are numerically superposed with different relative weights to describe the measured EPR spectrum of the spin-doped macrozwitterionic species Z. The calculations were performed on a DEC Alpha 3000−800 UNIX workstation (Digital Equipment Corp.) by a routine especially written for this purpose in the graphical-oriented language PV-WAVE (Visual Numerics Inc.). By systematically varying the relative weights of the three normalized subspectra, the program was designed to yield as a best fit the composed spectrum which exhibits the least standard deviation from the experimental spectrum. The consistency of this method was checked by performing the superposition on both differentiated and integrated spectra over a wide range of temperature and by varying the spectral range for which the standard deviation was to be determined by the computer program.

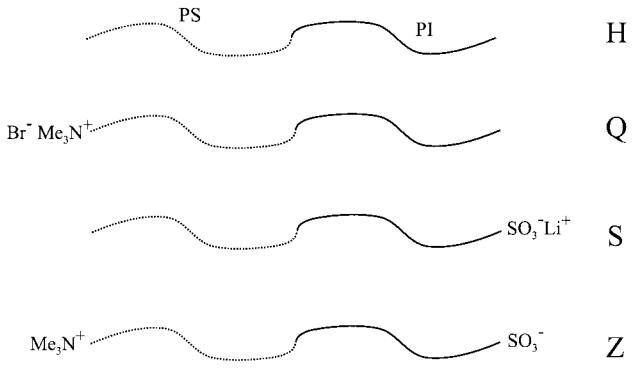

Figure 1. Schematic representation of the functionalized PS-*b*-PI diblock copolymers. H is the nonfunctionalized, S and Q the monofunctional, and Z the macrozwitterionic species.

Results

1. End-Capped Species. To investigate the influence of ionic chain ends on the self-assembly of diblock copolymers, well-defined materials with chain end functionality >95% and narrow MW distribution were used.[29] In this study four distinct species are considered, which are shown schematically in Figure 1 together with their code names. The neutral diblock with a dimethylamino group at the end of the PS block is termed H. In the case of single charged end-capped diblocks, either the PS block is functionalized with an quaternary ammonium bromide group (Q) or the PI block with a lithium sulfonate group (S). In an α,ω-macrozwitterionic diblock copolymer, Z, both ammonium and sulfonate groups are present. After synthesis the respective counterions Li^+ and Br^- are efficiently removed by dialysis (see Experimental Section). As checked by neutron activation analysis, this procedure washes out more than 99 mol % of the counterions. Our synthetic route allows one to obtain all four end-capped species from a single polymerization batch, i.e., MW distribution and PI microstructure are identical within one set of H, Q, S, and Z samples. Consequently, the impact of different ionic chain ends on the properties of these materials can be easily studied by direct comparison.

Symmetric diblocks of four different MWs in the range 11−49 kg/mol were synthesized. Their molecular characteristics are summarized in Table 1. In the following, the acronyms H, Q, S, and Z are used together with their MW in kg/mol, e.g., H11, Z49, etc.

2. Structure. 2.1. Static Structure: SAXS and TEM. TEM micrograph of S17, which is representative of what is observed for species S17, Q17, and H17, i.e. for monofunctional and neutral species of MW = 17 kg/mol, is shown in Figure 2a. A lamellar morphology is observed which corresponds to the classical behavior in the ordered state for $f \cong 0.5$.[35] The dialyzed, i.e., salt-free, macrozwitterion Z17 exhibits a completely different

Table 1. Molecular Characteristics of the End-Functionalized Block Copolymers[a]

sample	M_n (PS), g/mol	M_n (PS-*b*-PI), g/mol	M_w/M_n (PS-*b*-PI)	1,4-PI content, %	$f_{chain-ends}$, %
H,Q,S,Z11	5900	11000	1.13	28	>95
H,Q,S,Z17	8500	16500	1.10	27	>95
H,Q,S,Z24	12700	24000	1.09	29	>95
H,Q,S,Z49	25000	49000	1.08	28	>95

[a] Note that for each molecular weight four samples, H, Q, S, and Z, are obtained from one polymerization batch thus sharing the same molecular characteristics.

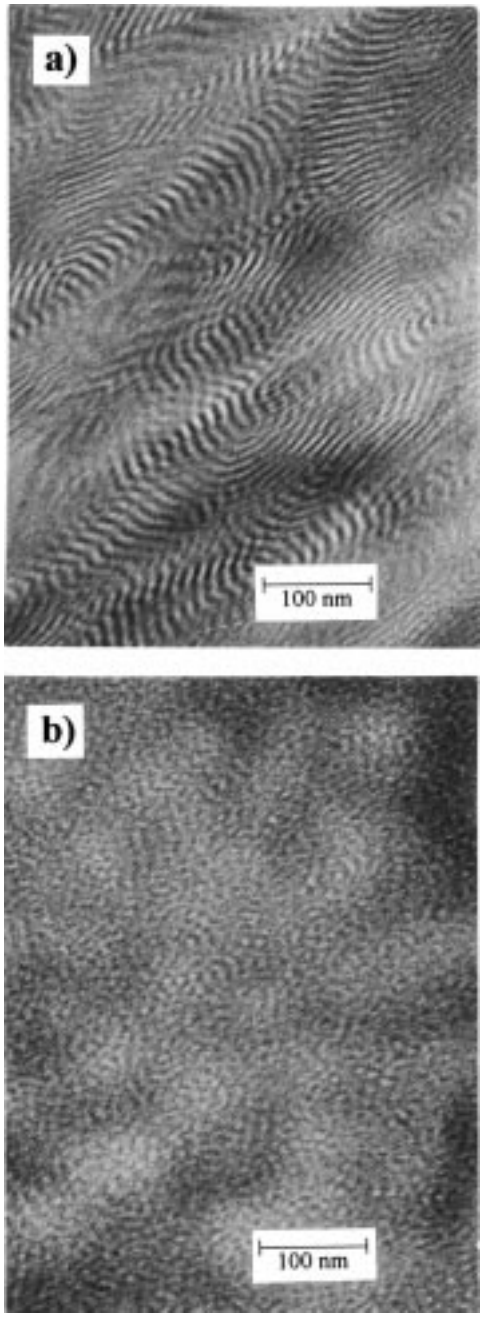

Figure 2. TEM micrographs of ionically end-capped PS-*b*-PI polymers: (a) S17, (b) Z17.

behavior. The TEM micrograph for this polymer shows a highly disordered structure (Figure 2b), reminiscent of a block copolymer melt in the disordered state, in which composition fluctuations on the length scale of the radius of gyration occur.[36] Note that the *chemical*

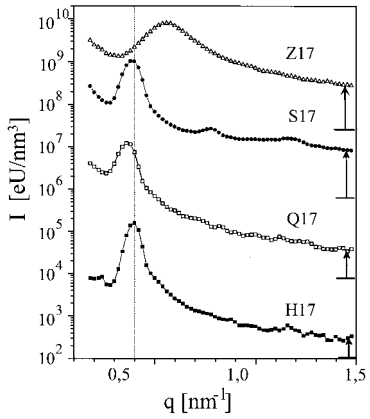

Figure 3. SAXS profiles of H17, Q17, S17, and Z17. The stack plot was obtained by multiplying the curves with a constant factor such that the dashed lines on the right-hand side of the figure correspond to the offset value 100 eU/nm^3, as given for H17. The arrows on the right-hand side visualize the scattering intensity above the respective offset lines.

difference between S17 (lamellar) and Z17 (nonlamellar) is only the quaternization of the amine group at the chain end of the PS block and the absence of low molecular weight counterions. The same significant changes in structure between Z17 and H17/Q17/S17 were also observed on samples which were obtained by casting from toluene solutions.

Structural differences between the end-capped species were further studied by SAXS: The diffraction patterns of H, Q, S, and Z (MW = 17 kg /mol) at room temperature are depicted in Figure 3 as a stack plot with a constant offset factor. In agreement with the TEM-pictures, S17 shows the characteristic Bragg peaks of a lamellar system at integer multiples of q^*, where q^* is the position of the first order maximum (much better developed as for H17 and Q17). Contrary to that, Z17 only shows a single broad peak which is typical for a block copolymer in an highly disordered state. Since q^* expresses the periodicity $L = 2\pi/q^*$ of the block copolymer system, the SAXS curves clearly manifest a significantly smaller value of L for Z17 compared to the neutral reference H17 (see dotted vertical line in Figure 3). On the other hand, both monofunctionals Q17 and S17 have slightly larger L than the reference H17. Note that corresponding to the TEM micrographs, L represents the spacing of *lamellae* in the case of H17, Q17, and S17 (cf. TEM), whereas for Z17, it indicates the length scale of *composition fluctuations* of a rather disordered system. Furthermore, from the height of the data points above the respective offset lines, indicated on the right-hand side of Figure 3, the samples S17 and Z17 exhibit significantly stronger scattering intensities at high scattering vectors ($q > 1.0$ nm^{-1}) than samples H17 and Q17. We attribute the additional scattering intensity in this q-range to the presence of ionic aggregates. For homopolymers, in which a regular arrangement of the ionic aggregates is possible, the so-called "ionomer peak" can be recognized in this q-range.[26] From SAXS studies on analogous end-capped homopolymers it was shown that the aggregates in S, containing sulfonate groups, give rise to a stronger scattering than the aggregates formed by the sample Q (quaternary ammonium bromide groups).[31]

The relative importance of the tendency toward microphase separation versus the formation of ionic aggregates can be changed by varying the degree of

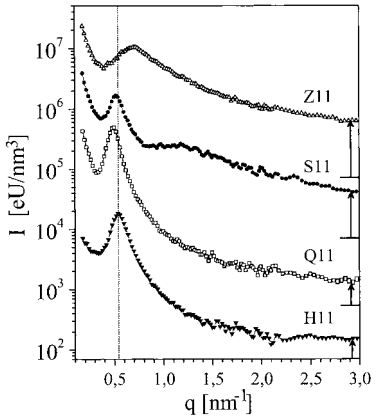

Figure 4. SAXS profiles of H11, Q11, S11, and Z11. The stack plot was obtained by multiplying the curves with a constant factor such that the dashed lines on the right-hand side of the figure correspond to the offset value 70 eU/nm^3, as given for H11. The arrows on the right-hand side visualize the scattering intensity above the respective offset lines.

polymerization N. For higher molecular weights the product χN increases and the number of chain ends decreases. The impact of ion aggregation upon self-assembly should therefore become less pronounced. Indeed, for the two series of samples of H, Q, S, and Z with MW = 24 and 49 kg/mol (cf. Table 1), lamellar structure was observed for *all* four species[30] (including Z24 and Z49), i.e., the classical morphology observed for symmetric diblocks. On the other hand, for lower N, ion aggregation should become more pronounced and dominate the behavior, particularly in the case of the salt-free macrozwitterion. Figure 4 shows the results of SAXS measurements on a series of samples with a MW of 11 kg/mol: H11, Q11, S11, Z11. For S11 the ionic aggregates contribute strongly to the scattering intensity—for this MW a broad ionomer peak with its center around 1.2 nm^{-1} is observed. For this species ionic aggregates and composition fluctuations due to the diblock copolymer structure seem to be well accommodated. It is interesting to note that for the macrozwitterionic species Z11 both structural features superimpose and seem to be blurred. As for S11, there is a strong scattering signal for $q \geq 1.0$ nm^{-1} but no distinct ionomer peak can be recognized. Compared to the neutral and monofunctional species, the block copolymer peak is shifted toward larger q-values and is significantly broadened. Apparently, both self-assembly mechanisms compete with each other, thus leading to neither a well-defined composition fluctuation nor to regularly distributed ionic aggregates.

For a more detailed analysis in Figure 5 the periodicity $L = 2\pi/q^*$ (a) and the full width at half-height (fwhh) (b) of the main peak in the SAXS data are shown. Values of 2π/fwhh correspond to a length over which the fluctuations leading to the peak are correlated. For the determination of fwhh a flat background in $I(q)$ was taken into account.

The double logarithmic representation of Figure 5a yields $L \propto \mathrm{MW}^{0.62}$ for the neutral diblocks, i.e., the familiar deviation from the Gaussian behavior in segregated block copolymers.[37,38] Note that all values for the macrozwitterion Z are about 25% smaller than those obtained for the analogous H-species, while the data of the monofunctional species Q and S are systematically larger than those of H by about 5%. Since from the synthesis the MW characteristics are identical for each

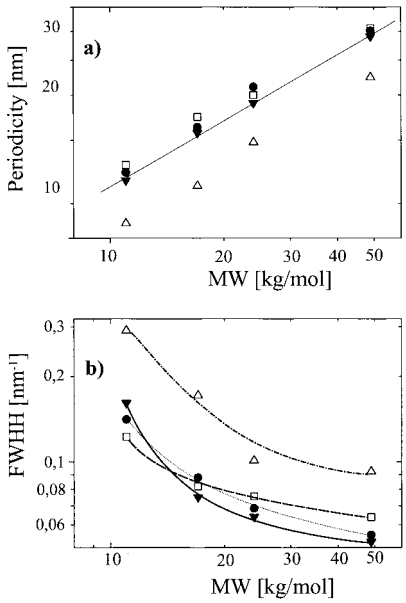

Figure 5. Periodicity $L = 2\pi/q^*$ (a) and fwhh = full width at half-height (b), as obtained from the SAXS profiles for H (▼), Q (□), S (●), and Z (△) as a function of molecular weight. The lines connecting the data points serve as a guide to the eye.

set of H/Q/S/Z samples, the significant differences shown in Figure 5a can only be attributed to conformational changes of the block copolymer chains in the bulk due to the presence of charges. We will come back to the discussion of this effect after presentation of the EPR results.

Comparison of values for fwhh plotted in Figure 5b demonstrates that Z suffers a pronounced loss of long-range order compared to the other species within a given set of end-capped diblocks. This effect is consistent with the observed differences as demonstrated by the TEM micrographs in Figure 2. Due to the difficulty in performing background subtraction in the case of the very broad peak of Z11, there is some uncertainty in the large fwhh value for this sample. Note that the domain size is much less affected in the case of the monofunctional species. Comparison of the data points for Q and S with those of H reveals a weak loss in the long-range order for the monofunctionals of MW ≥ 17 kg/mol. For the low molecular weight samples H,Q,S11, the situation is inverted: The higher correlation length for Q11 and S11 relative to H11 suggests that in the weak segregation regime the presence of a single ionic chain end improves microphase separation and thus induces additional long range order. The difference in fwhh for the monofunctionals Q und S indicate a stronger MW dependence for the sulfonated species i.e., a stronger interplay between microphase separation and ion aggregation compared to the ammonium-capped species (see crossover above MW = 17 kg/mol).

2.2. Temperature-Dependent SAXS. Next, the impact of ionic chain ends on the temperature dependence of the SAXS patterns is examined for the end-capped block copolymers. Only data for samples with MW = 17 kg/mol will be discussed, since for this MW the ODT of the neutral species lies within an experimentally accessible temperature window. Besides H17 and Z17, S17 will be taken as an example for the monofunctional species.

The reciprocal intensity at q^* [$I^{-1}(q^*)$] and fwhh are plotted against T^{-1} in parts a and b of Figure 6,

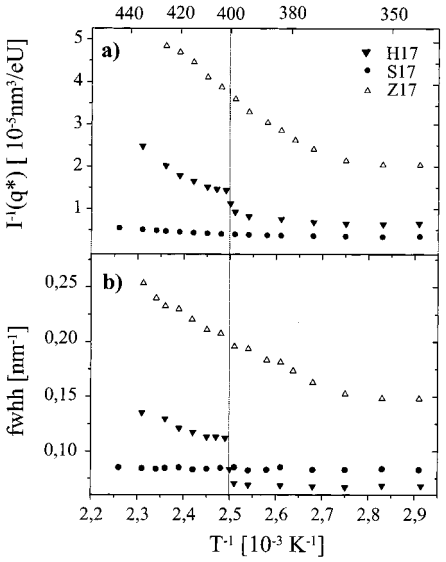

Figure 6. Inverse intensity $I^{-1}(q^*)$ (a) and fwhh = full width at half-height (b) vs inverse temperature for the microphase separation peak of H17 (▼), S17 (●), and Z17 (△).

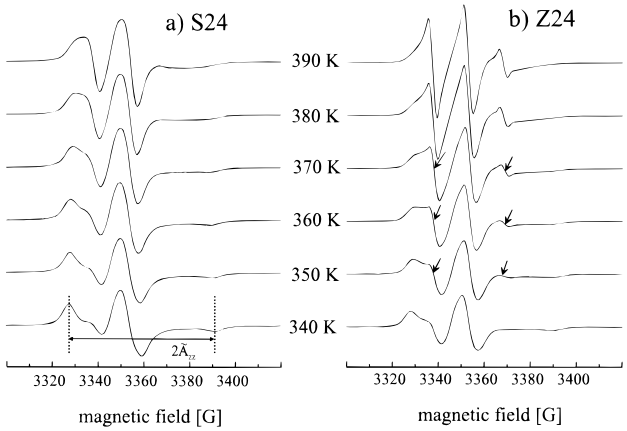

Figure 7. EPR spectra of S24 (a) and Z24 (b) doped with K-TEMPO as a function of temperature. At the bottom of part a, for the lowest temperature, the outer extrema separation $2\tilde{A}_{zz}$ is indicated. In part b arrows denote the outer extrema separation of the fast dynamical component.

respectively. In the case of the nonionic diblock H17, a discontinuity in $I^{-1}(q^*)$ and fwhh shows up at 400 K, which corresponds to the classical ODT signature.[39,40] Considering the monofunctional lamellar diblock S17, however, the peak intensity and peak width are almost constant over the whole temperature range. There is thus neither signature for an ODT nor evidence for any enhanced microphase mixing with increasing temperature. Similarly, in a recent work by Floudas et al., stabilization of microdomains up to high temperatures was observed for asymmetric PS-*b*-PI's, *ω*-functionalized with a sulfobetaine group.[41,42] For the macrozwitterion Z17, on the other hand, both fwhh and $I^{-1}(q^*)$ are much larger compared to that for H17 and increase with increasing temperature. This behavior indicates that on raising the temperature, a progressive deterioration of block segregation and long-range order occurs, in strong contrast to S17.

In summary, structural data as obtained from TEM and SAXS measurements show that the presence of ionic chain ends gives rise to two major effects on the block copolymer structure: (a) Compared to the neutral species H, the block copolymer periodicity becomes significantly smaller in the case of the macrozwitterion Z, whereas it slightly increases for the monofunctional species Q and S. (b) The presence of the ionic chain ends strongly stabilizes the microphase separated state for monofunctional diblock copolymers, whereas for the salt free macrozwitterionic diblock copolymers the formation of microdomains is heavily perturbed (destabilization).

3. Localization of Ion Aggregates: EPR. To account for the significant structural changes observed by SAXS, it is essential to characterize the association behavior of the ionic chain ends. To this end, we recently introduced a simple spin probe experiment which allows to characterize the dynamics of ionic aggregates in telechelic ionomers by EPR spectroscopy.[31] The experiment relies on the fact that an ionic paramagnetic probe, when incorporated in a polymer containing only a few ionic moieties, will preferentially reside close to these ionic groups.[43] From the extrema separation of the temperature-dependent EPR spectra, a characteristic temperature T'_{50G} can be derived, which serves as a measure for the association tendency of a specific end group in a given polymer matrix.[31] Such a tool is particularly useful when the fraction of ionic groups is small and thus difficult to "visualize" by scattering experiments. In a first study we concentrated on model mono- and bifunctional PS and PI homopolymers and demonstrated that the main factors governing the dynamics of multiplets are the chemical type of ionic end group and the nature of the polymer backbone.[31] On the basis of the EPR characterization of the respective homopolymers, we will now extend this study to the present end-capped diblock copolymers.

To this end, Q, S, and Z were doped with the ionic probe K-TEMPO (potassium salt of 4-carboxy-TEMPO). After annealing, temperature-dependent CW-EPR spectra were recorded. Representative spectra of S24 and Z24 are depicted in parts a and b of Figure 7, respectively. The TEMPO spectrum exhibits a characteristic three line pattern due to the hyperfine coupling of the electron spin with the nuclear spin of ^{14}N. When rotational diffusion of the probe is slow, the anisotropy of the coupling tensor *A* gives rise to three broad lines with an outer extrema separation $2\tilde{A}_{zz} \cong 65$ G, as indicated on the bottom of Figure 7a. At higher temperatures, when rotational motion of the probe becomes sufficiently rapid, the anisotropies of the hyperfine interactions are averaged out, giving rise to a narrowing of the whole spectrum, reflected in a decrease of the outer extrema separation. The transition from the slow tumbling case ($2\tilde{A}_{zz} \cong 65$ G) to the motionally narrowed spectrum can be characterized by a temperature T_{50G} where the outer extrema separation is 50 G. Since T_{50G} is commonly used as a parameter which is related to the glass transition of a polymer, we introduced T'_{50G} for the *ionic* probe in order to distinguish between matrix mobility and dynamics of ion aggregates.[31]

3.1. Monofunctional Diblock Copolymers. First, consider the monofunctional species S24 in Figure 7a, i.e., the copolymer bearing lithium sulfonate groups at the end of the PI block. With increasing temperature motional narrowing of the spectrum is observed. Around 390 K the extrema separation reaches the characteristic value of 50 G and further decreases upon heating. To relate this behavior with ionic clustering in an end-capped PI homopolymer, the extrema separation $2\tilde{A}_{zz}$ is plotted over a wide temperature range in Figure 8 together with $2\tilde{A}_{zz}$ values obtained for a sulfonated PI

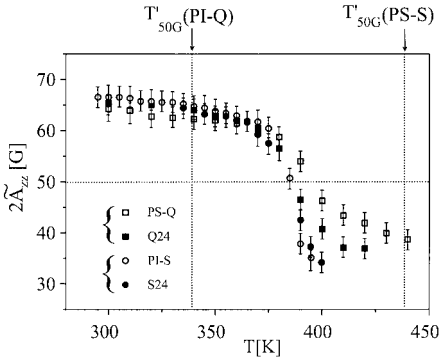

Figure 8. Extreme outer peak separation $2\tilde{A}_{zz}$ vs temperature for the monofunctional species PS-Q (□), Q24 (■), PI-S (○), and S24 (●). An error bar of 2 G is assumed for all spectra. As references the temperatures at which the outer extrema separation for the two samples PI-Q and PS−S reach 50 G are indicated by vertical lines (see text).

Table 2. Glass Transition Temperatures and T'_{50G} Values of the End-Functionalized Block Copolymers

sample	T' (PI), K	T_g (PS), K	T'_{50G}, K
H11	278	334	
Q11	277	343	378
S11	283	332	388
Z11	(283)		*a*
H17	272	350	
Q17	272	359	383
S17	274	349	390
Z17	281	345	*a*
H24	264	355	
Q24	264	359	382
S24	265	355	385
Z24	268	347	*a*
H49	259	369	
Q49	261	368	
S49	260	368	
Z49	262	367	

[a] Contains several dynamic components, see section 3.2.

homopolymer (PI-S).[29,31] The anionic polymerization procedure by which the lithium sulfonate group has been attached to the PI chain end is identical for PI-S and S24.[31] Hence, identical microstructure is assured for the PI units (1,4 content of ca. 28%, cf. Table 1). A sigmoidal curve $2\tilde{A}_{zz}(T)$ with an inflection point at $T'_{50G} \approx 385$ K is obtained for both S24 and PI-S. From these data two important conclusions can be drawn:

1. Considering that T'_{50G} is about 100 K above the PI glass transition temperature (cf. Table 2) the dynamics of K-TEMPO can only be accounted for by the presence of highly immobilized ionic aggregates to which the spin probe is anchored. Hence, ion clustering occurs in both monofunctional species, sulfonated homopolymer and block copolymer.

2. The coincidence of T'_{50G} for PI-S and S24 reveals that K-TEMPO is located in the same dynamical environment in both samples. Having demonstrated in our previous work that T'_{50G} is sensitive not only to the nature of ionic endgroup but also to T_g of the surrounding polymer matrix, the data for the monochelic S24 can only be interpreted by lithium sulfonate aggregates located in a *pure* PI microphase. For comparison, as indicated by a vertical line in Figure 8, T'_{50G} of lithium sulfonate aggregates in a PS matrix (PS−S) was found at much higher temperatures (ca. 430 K).[31]

Similarly, the association of ammonium bromide chain ends of the PS block was investigated. In this case, the diblock Q24 is compared with a PS homopolymer, end-capped with the same ammonium bromide moiety (PS-Q).[31] The $2\tilde{A}_{zz}$ values as obtained from temperature-dependent CW-EPR spectra of both polymers are also plotted in Figure 8. Just as above, the two curves almost coincide. At the same time the value of T'_{50G} extracted from these data is again about 385 K as in the case of S24 and PI-S. In analogy to the sulfonate-capped species discussed above, the data reveal that for the monofunctional diblock Q24 ammonium bromide aggregates are located in the *pure* PS phase. As indicated in Figure 8 by a vertical line, ammonium bromide aggregates dispersed in a PI phase (PI-Q) give rise to a much lower T'_{50G} (ca. 335 K) due to the lower T_g of PI relative to PS. The coincidence of T'_{50G} values for S24 (PI-S) and Q24 (PS-Q) is thus rather accidental. It is due to the fact that in S24 a strong dipole (lithium sulfonate) is attached to a low T_g polymer backbone, whereas in Q24, a rather weak dipole (ammonium bromide) is attached to a high T_g polymer. Similar behavior of the ionic spin probe was observed for all monofunctional diblocks of varying MW investigated in the present study. Results for T'_{50G} are summarized in Table 2 together with the glass transition temperatures as determined by DSC.

3.2. Macrozwitterionic Diblock Copolymers. Next, consider the case of the bifunctional polymers Z. This situation is particularly interesting and indeed for these species the most significant differences in the SAXS pattern were found relative to the neutral diblock H. Since the macrozwitterions were dialyzed thoroughly, obtaining a rest ion content of less than 1% of the initial ion concentration, aggregation of different chain ends is expected to occur preferentially in the interface between PS and PI, to achieve charge compensation. The spin probe spectra obtained from Z should therefore provide valuable information about the dynamics of the aggregates in these macrozwitterionic species.

A representative series of CW-EPR spectra of Z24 doped with K-TEMPO as a function of temperature is plotted in Figure 7b. Above 340 K, the lowest temperature in the stack plot, a fast dynamical component with line splitting of roughly 30−40 G, indicated by arrows, can clearly be identified besides a slow dynamic component with outer extrema separation of about 60 G. Note that the fast component is not at all present in the EPR spectra of the monofunctional species (cf. Figure 7a) and hence suggests a partially mobilized and, thus, *heterogeneous* dynamical environment of the spin probe.

To get a quantitative measure of the different dynamical components which occur in the EPR spectra of Z24, numerical simulations of these spectra would need to be performed. A full analysis would require modeling of all EPR spectra in terms of all magnetic parameters such as *g*-tensors and hyperfine tensors, line width, line shapes, and specific motional models.[44,45] This is far beyond the scope of the present paper. However, there is a much simpler way for a *semiquantitative* analysis of such a complex system. The bimodal distribution of rotational correlation times reflected in the experimental spectra suggests simulation of the spectra by a superposition of experimental spectra, representing components of different mobility. From Figure 7b, there is clearly one "slow component" I, which is similar to what is observed for polymer S24 (compare parts a and b of Figure 7) and, additionally, a component

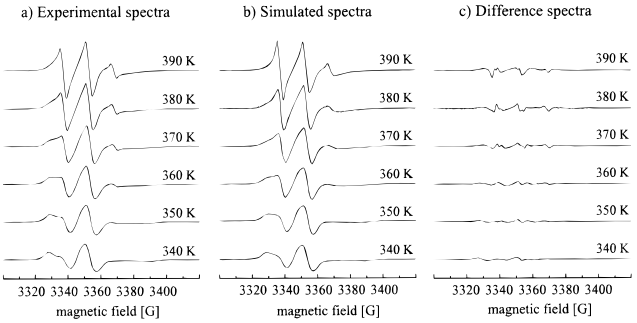

Figure 9. Comparison of composite EPR spectra of Z24 (b), obtained by superposition of three subspectra I, II, and III with experimental EPR-spectra of Z24 (a) as a function of temperature. In (c) the difference spectra of (a) and (b) are shown. Within the entire temperature inverval the portion of the components I, II, and III is 30−40, 50−60, and 0−10%, respectively.

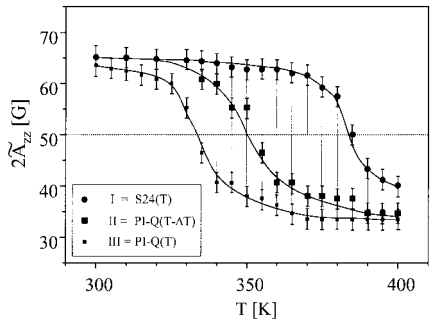

Figure 10. Extreme outer peak separation $2\tilde{A}_{zz}$ vs temperature of components I, II, and III as used in the superposition for the composite spectra shown in Figure 9b. An error bar of 2 G is assumed for all spectra. Lines connecting the data points serve as guide to the eye. For all temperatures, the portion of the components I, II, and III is 30−40, 50−60, and 0−10%, respectively.

II of significantly higher mobility. Since within our homopolymer data only PI-Q exhibits similar high mobility, we first superposed temperature dependent normalized experimental spectra, S24(T) and PI−Q(T), with varying relative weights w(I) and w(II). Indeed, good agreement between such simulated spectra and the experimental line shapes of Z24 for all temperatures was obtained by superposition of almost equal amounts of S24(T) and PI-Q($T-\Delta T$), allowing a temperature shift ΔT of ca. 20−30 K between the two components:

$$\text{Z24}(T) = w(\text{I})\text{S24}(T) + w(\text{II})\text{PI-Q}(T\text{-}\Delta T); \quad 20\ \text{K} \le \Delta T \le 30\ \text{K}; \quad w(\text{I}) + w(\text{II}) = 1 \quad (1)$$

An even better agreement was obtained by considering a small fraction of a third component III with weight w(III) < 0.1 with a mobility close to that of PI-Q(T), i.e., the set of experimental spectra at the same temperature as S24(T):

$$\text{Z24}(T) = w(\text{I})\text{S24}(T) + w(\text{II})\text{PI-Q}(T-\Delta T) + w(\text{III})\text{PI-Q}(T); \quad 20\ \text{K} \le \Delta T \le 30\ \text{K}; \quad w(\text{I}) + w(\text{II}) + w(\text{III}) = 1 \quad (2)$$

The good agreement between the simulations on the basis of eq 2 and the experimental line shapes is demonstrated in Figure 9. Our semiquantitative analysis of the EPR spectra of Z24 requires a minimum of adjustable parameters. The weighting parameters are essentially constant for the whole series: It is 30−40% for the rigid component I, 50−60% for the dominant component II, and 0−10% for the highly mobile component III. The motional heterogeneity reflected in the spin probe spectra is visualized in Figure 10 where the temperature dependence of the $2\tilde{A}_{zz}$ values for the different components used in the simulation are plotted. All three components exhibit the characteristic narrowing, but at different temperatures. The two main components clearly show that the heterogeneous dynamical behavior of the spin probe, as introduced above in a qualitative interpretation of the experimental spectra, is in fact mainly bimodal in character with a small extension of the mobile part to even higher mobility.

Compared to our data on ionically end-capped homopolymers the temperature dependence for the major mobile component II corresponds to that of aggregates formed by macrozwitterionic PI's (PI-Z), i.e., mixed aggregates consisting of associating ammonium and sulfonate end groups in a PI matrix.[31] Indeed, their T'_{50G}(PI-Z) ≅ 355 K agrees well with what is observed for component II in Figure 10. This, in turn, suggests that in the macrozwitterionic diblock species Z24 mixed aggregates occur, thus creating an additional microdomain interface which is strongly plasticized by the rubbery PI phase.[46] According to this interpretation, we think that the proximity of components II and III, as derived from the fitting, simply accounts for the local distribution of mixed aggregates within the plasticized interfacial layer. Component I, on the other hand, evidences the presence of aggregates of restricted mobility owing to the pronounced mobility gradient between PI and highly immobilized PS domains. It is also in agreement with recent experiments that small amounts of low molecular salt can efficiently suppress aggregation of macrozwitterionics,[30] as shown schematically by the equilibrium

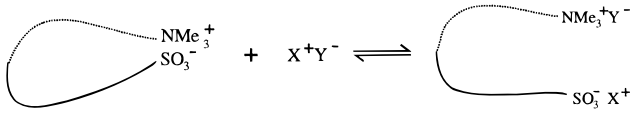

Small amounts of salt (residual LiBr, K-TEMPO, glassware) are likely to prevent chain end association at the interfacial region and thus partially contribute to multiplet formation in the pure microdomains (cf. $T'_{50G} \approx 385$ K corresponds to what is observed for both monofunctional species, see Figure 8).

We conclude from EPR that ion aggregates are localized within pure microdomains in the case of monofunctional diblock copolymers (Q, S) whereas in the macrozwitterionic diblock Z, oppositely charged chain ends form aggregates that are heterogeneously distributed in the microdomain interface. These EPR results on ion aggregation are summarized pictorially in Figure 11 including the differences in domain spacing as found by SAXS ($L_{Q,S} > L_Z$). The consequences on chain topology which can be derived from our experimental results will now be discussed in more detail.

Discussion

Having localized ionic aggregates within distinct microphases by EPR we will now relate these results to our SAXS data. As shown in Figure 5, a systematic change in domain spacing L was found for all species of a given molecular architecture: a decrease in periodicity $L_Z/L_H \cong 0.75$ for the macrozwitterions and a

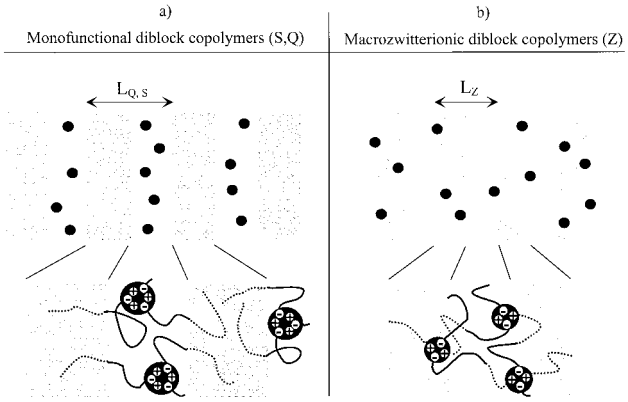

Figure 11. Schematic representation of the self-assembly in ionically end-capped diblock copolymers. (a) Monofunctional diblocks Q and S where ion aggregation of the chain ends occurs within the pure homopolymer phases and (b) α,ω-macrozwitterionic species Z where ionic chain ends aggregate, creating a large microdomain interface. In the bottom picture, both looping and bridging are schematically depicted.

slight increase for the monofunctional species ($L_{Q,S}/L_H \cong 1.05$). Since the composition and total degree of polymerization is identical for all species within one set of H, Q, S, and Z samples, the shifts in domain spacing can only be attributed to a conformational change of the macromolecules.

The data indicate that for sample Z ionic aggregation leads to considerable looping of chains as depicted schematically in Figure 11b. This is similar to $(AB)_n$ multiblock copolymers, in which substantial looping besides bridging occurs.[47−49] The extreme case of pure looping was investigated on cyclic *di*block copolymers, where L was reduced by a factor of 0.91−0.95 relative to the linear *tri*block of the same degree of polymerization N and composition f.[50] In multiblocks loops occur in order to minimize the entropic penalty which is associated with bridging where the chain is considerably stretched along the lamellar normal. Unfortunately, no experimental data are available for direct comparison of cyclic with linear *di*blocks. An estimation for the reduction in domain spacing of 0.60−0.62, however, is given by theory.[49] This change in periodicity, for a fixed N and f, is indicative of an increase in compatibility between the two polymers, as illustrated schematically in the vertical direction on the left-hand side of Figure 12. Therein, the abscissa indicates the number of trivalent or higher grafting points per molecule which is zero in the case of linear species. Starting from a simple A−B diblock at the bottom left, the compatibility is increased by increasing the fraction of bivalent junctions per total number of blocks (one-half for a diblock, two-thirds for a triblock, etc. and 1 for a cyclic or a multiblock with "infinite" block number).

The self-assembly of Z is more complicated than in cyclic diblocks or multiblocks: By considering ion multiplets as (thermoreversible) branching points, where the ionic chain ends are joined via electrostatics, the end-capped block copolymers should rather be compared to graft or star copolymers. Following this analogy, the average aggregation number of ion multiplets corresponds to the arm number of a star block.

First consider Z: Since for entropic reasons bifunctional telechelics preferentially bridge between ionic multiplets,[51] it can be expected that the macrozwitterions constitute a network of ionic cross-links which are interconnected by diblock copolymer chains. Therefore, the observed enhanced microphase mixing should be compared to that of star block copolymers with chemically different arms. From the large number of architectures described in the literature, only a few representative examples are shown in Figure 12 and compared with the present system. Note that Figure 12 serves as a very qualitative picture. The position of the individual species within the diagram could only be roughly estimated from literature data.[8,9,11,46,49] Since grafting costs additional stretching energy of the chains due to crowding at the interface,[52] the microphase-separated state becomes destabilized (increased compatibility) with respect to the linear species.[53] This is obviously the case for salt-free macrozwitterionic diblocks, where considerable crowding at the interface occurs, because *all* chain ends are "grafted" at starlike *mixed* ion multiplets. Following Hadjichristidis' nomenclature,[9] the present macrozwitterionics correspond to a network of a polydisperse miktoarm star block copolymer. A high similarity exists between Z and the inversed 4-miktoarm star shown in Figure 12 but no morphological studies have so far been published.[11]

In the case of the monofunctional species Q and S, ion aggregates slightly *increase* the periodicity. As evidenced by EPR, chain ends only associate in the pure phases and microphase separation is significantly stabilized. Following the comparison with covalently branched block copolymers and according to the illustration in Figure 11a, this system corresponds to a star block copolymer with n identical arms of AB diblocks. A schematic representation of this "star polymer" is included in Figure 12. The effect of the arm number n on the morphology of such star-branched blocks for *constant* arm length and composition was found to be rather small,[54] but a slight increase in periodicity by the factor ≅1.10 has been established for all species with $n \geq 2$, relative to the linear diblock.[55] This linkage is achieved by ion multiplets in the respective pure microdomain for Q and S. Note that $n = 2$ simply corresponds to a triblock which is linked by two diblocks following

This case has been investigated in an early study using SAXS.[35] Therein, the authors claim to find no pronounced difference between the triblocks and the diblocks of half the molecular weight, although *all* their experimental data points on the lamellar spacing show slightly higher values for triblocks than for the corresponding diblocks—in the range of a few percent. A more recent rheological study has shown that triblocks have a significantly higher ODT than their half-molecular weight precursor diblock, indicating a higher degree of block segregation.[56] Theoretical examination of microphase separation of starblock copolymers with monodisperse diblock arms showed that the triple point in the phase diagram is indeed shifted from the classical value for diblocks $\chi N \cong 11$ to ca. 8.5 and 7.5 for $n = 3$ and 5, respectively.[57] Concomitantly, an increase in lamellar spacing of the order of a few percent is predicted, as also observed in the present ionically joined "star block copolymers" Q and S.

The comparison with covalently linked copolymer structures nicely fits with the observed morphological differences between the ionically end-capped species, as indicated on the "compatibility scale" shown in Figure

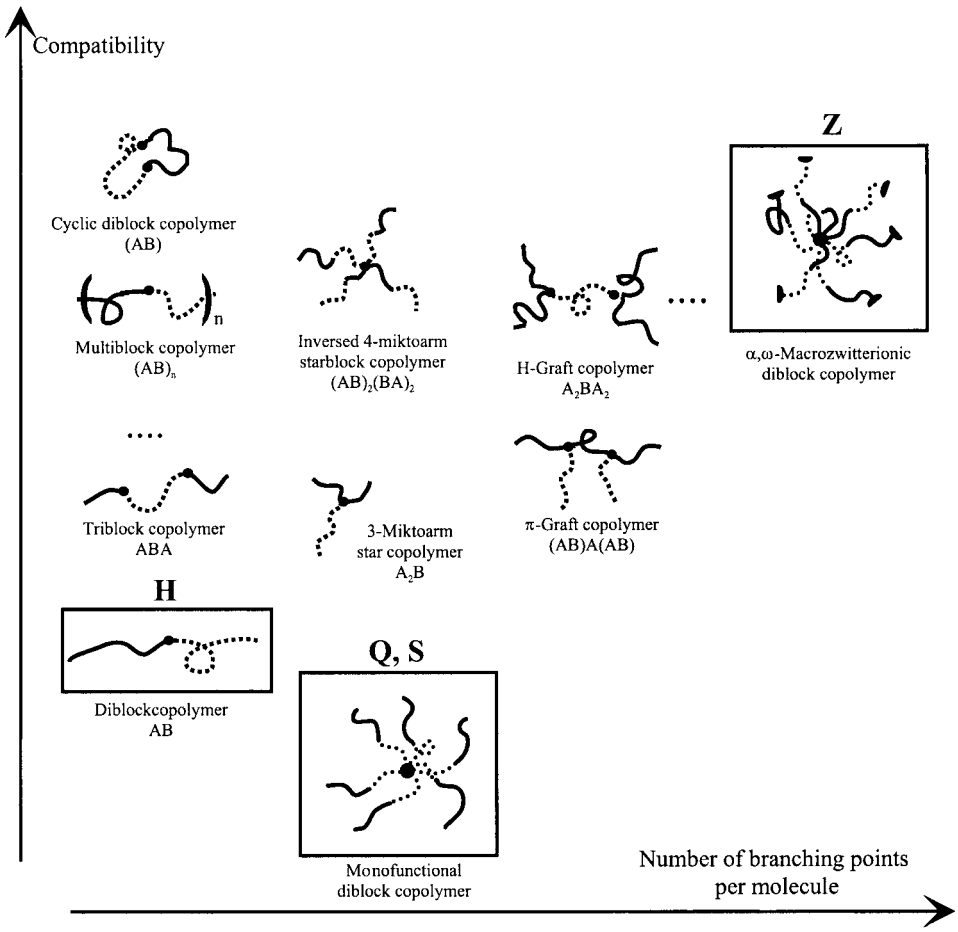

Figure 12. Schematic representation of some block copolymer architectures: The diagram shows trends in compatibility by changing the molecular architecture for a fixed degree of polymerization and composition. When the monofunctionals Q and S or the macrozwitterion Z are compared with H, it should be noted, however, that the ionically end-capped species give rise to ionically joined "star polymers" with arms the size of the corresponding H species, hence of much higher total molecular weight.

12. This can only be a first-order approximation, however, since a full description of the phase behavior of these materials would have to take into account further contributions to the total free energy arising from ion aggregation.[58] This would certainly be an ambitious task and is beyond the scope of the present paper.

Conclusions

The experimental results on ionically end-capped diblock copolymers of well-defined chemical structure demonstrate that such materials represent ideal model systems which enable the study of competition between block copolymer microphase separation and aggregation of ionic chain ends. In the present system the interference of these "tandem molecular interactions" gives rise to a strong alteration of the block copolymer morphology and phase behavior, as evidenced by SAXS and TEM: The microphase periodicity (lamellar spacing) is significantly decreased in the case of salt-free α,ω-macrozwitterionic diblock copolymers, whereas in the case of the ω-functionalized diblocks, the spacing is slightly increased. As shown by an EPR spin probe technique, using a paramagnetic probe which is selectively sensitive to the dynamics of ionic aggregates, these structural differences can clearly be attributed to the presence of ionic aggregates within different microdomains:

For ω-functionalized diblock copolymers association of ionic chain ends occurs within the pure microdomains, thus stabilizing the block copolymer microphase separation; in contrast, for α,ω-macrozwitterionic diblock copolymers, association of ionic chain ends gives rise to enhanced mixing of unlike segments, hence, microphase separation is strongly suppressed. The aggregation of ions in the case of the monofunctionals can be viewed as formation of an ionically linked star block copolymer, where the arm number is given by the functionality of the ion multiplet. On the contrary, a network of mixed multiplets which are connected via diblock bridges is formed in the case of the α,ω-functionalized species. Comparison with analogous copolymer architectures reveals that a change in compatibility is observed for the corresponding graft copolymers, i.e., a decrease and increase of compatibility for the ω-functionalized and α,ω-macrozwitterionic species, respectively.

These results reveal that controlled introduction of ionic interactions in specifically functionalized block copolymers offers a unique possibility for altering the morphology of a block copolymer system in the bulk. Contrary to the concept of morphology manipulation by introducing covalent bonds to the polymer chain (e.g., chlorosilane chemistry for constructing graft and star block copolymers), the use of ionic interactions can be employed in a *reversible* way, since ionic aggregation can be further controlled, e.g., by the presence of salts.[30]

Since the concept of screening ionic interactions by salt is borrowed from the study of polyelectrolytes in solution, one can expect that similar effects are also

observed for the self-assembly of the present model block copolymers in a selective solvent. Indeed, in a recent publication we have reported on the first results of the effect of electrostatics in the micellization of these macromolecular surfactants.[59] More experimental work on the self-assembly of ionically functionalized block copolymers in bulk and solution is now in progress in our laboratory.

Acknowledgment. We acknowledge Dr. G. Lieser, G. Weber, and Dr. Y. Zhang for the TEM-micrographs and Dr. Trautmann (Institut für Kernchemie, Johannes Gutenberg-Universität, Mainz) for carrying out the neutron activation analysis. We further thank A. Franck for his skillful support during the polymer synthesis, the EPR group for technical assistance with the CW spectrometer, and Ute Pawelzik for the DSC measurements. We are furthermore indebted to Prof. Hadjichristidis for stimulating discussion. The financial support from the Deutsche Forschungsgemeinschaft (DFG-Schwerpunkt Polyelektrolyte) and the Studienstiftung des deutschen Volkes for a scholar (V.S.) are gratefully acknowledged.

References and Notes

(1) Richards, D. H.; Swarc, M. *Trans. Faraday Soc.* **1959**, *55*, 1644.
(2) Fredrickson, G. H.; Bates, F. S. *Annu. Rev. Mater. Sci.* **1996**, 26, 501. Whitmore, M. D.; Vavasour, J. D. *Acta Polym.* **1996**, *46*, 341.
(3) Hillmyer, M.; Bates, F.; Almdal, K.; Mortensen, K.; Ryan, A.; Fairclough, J. P. A. *Science* **1996**, *271*, 976.
(4) Leibler, L. *Macromolecules* **1980**, *13*, 1602.
(5) Khandpur, A. K.; Förster, S.; Bates, F. S.; Hamley, I. W.; Ryan, A. J.; Bras, W.; Almdal, K.; Mortensen, K. *Macromolecules* **1995**, *28*, 8796.
(6) Matsen, M. W.; Bates, F. S. *Macromolecules* **1996**, *29*, 7641.
(7) Gido, S. P.; Lee, C.; Pochan, D. J.; Pispas, S.; Mays, J. W.; Hadjichristidis, N. *Macromolecules* **1996**, *29*, 7022.
(8) Tselikas, Y.; Hadjichristidis, N.; Lescanec, R. L.; Honeker, C. C.; Wohlgemut, M.; Thomas, E. L. *Macromolecules* **1996**, *29*, 3390.
(9) Iatrou, H.; Hadjichristidis, N.; *Macromolecules* **1992**, *25*, 4649. Hadjichristidis, N. et al. *Macromolecules* **1993**, *26*, 5812.
(10) Floudas, G.; Hadjichristidis, N.; Iatrou, H.; Pakula, T.; Fischer, E. W. *Macromolecules* **1994**, *27*, 7735.
(11) Hadjichristidis, N.; Tselikas, Y.; Iatrou, H.; Efstratiadis, V.; Avgeropoylos, A. *J. Macromol. Science—Pure Appl. Chem.* **1996**, *A33* (10), 1447.
(12) Stadler, R.; Auschra, C.; Beckmann, J.; Krappe, U.; Voigt-Martin, I.; Leibler, L. *Macromolecules* **1995**, *28*, 3080.
(13) Beckmann, J., Auschra, C., Stadler, R. *Macromol. Chem., Rapid Commun.* **1994**, *15*, 67.
(14) Krappe, U.; Stadler, R.; Voigt-Martin, I. *Macromolecules* **1995**, *28*, 4558. Breiner, U.; Krappe, U.; Abetz, V.; Stadler, R. *Macromol. Chem.* **1997**, *198*, 1051.
(15) Balsamo, V.; von Gyldenfeldt, F.; Stadler, R. *Makromol. Chem. Phys.* **1996**, *197*, 1159.
(16) Adams, J., Gronski, W. *Macromol. Chem. Rapid Commun.* **1989**, *10*, 553.
(17) Mao, G.; Ober, C. K. *Acta Polym.* **1997**, *47*, 405.
(18) NATO Advanced Research Workshop*: Manipulation of Organization in Polymers using Tandem Molecular Interactions*; Il Ciocco, Italy; May 29—June 2, 1996, *Macromol. Symp.* **1997**, *117*, 7.
(19) Chen, J. T.; Thomas, E. L.; Ober, C. K.; Mao, G.-P. *Science* **1996**, *273*, 343.
(20) Wang, J.; Mao, G.; Ober, C. K.; Kramer, E. J. *Macromolecules* **1997**, *30*, 1906.
(21) Chiellini, E.; Galli, G.; Angeloni, A. S.; Bignozzi, M. C.; Laus, M.; Sehatli, E. I.; Yagci, Y. *Polym. Prepr. (Am. Chem. Soc., Div. Polym. Chem.)* **1993**, *34*, 190.
(22) Angeloni, A. S.; Bignozzi, M. C.; Laus, M.; Chiellini, E.; Galli, G. *Polym. Bull.* **1993**, *31*, 387.
(23) Galli, G.; Chiellini, E.; Yagci, Y. Serhatli, E. I.; Laus, M.; Bignozzi, M. C.; Angeloni, A. S. *Macromol. Chem. Rapid Commun.* **1993**, *14*, 185.
(24) Galli, G.; Chiellini, E. *Makromol. Chem. Phys.* **1994**, *195*, 2247.
(25) See, e.g.: Schlick, S., Ed. *Ionomers, Characterizaion, Theory, and Applications*; CRC Press: New York, 1996; Chapter 1.
(26) Williams, C. E.; Russell, T. P.; Jérôme, R.; Horrion, J. *Macromolecules* **1986**, *19*, 2877.
(27) e.g.: Völkel, T.; Zweifel, H. *Makromol. Chem.* **1973**, *170*, 141. Eisenbach, C. D.; Schnecko, H.; Kern, W. *Makromol. Chem.* **1975**, *176*, 1587.
(28) Antonietti, M.; Heyne, J.; Sillescu, H. *Makromol. Chem.* **1991**, *192*, 3021.
(29) Schädler, V.; Spickermann, J.; Räder, H.-J.; Wiesner, U. *Macromolecules* **1996**, *29*, 4685.
(30) Schädler, V.; Wiesner, U. *Macromolecules* **1997**, *30*, 6698.
(31) Schädler, V.; Franck, A.; Wiesner, U.; Spiess, H. W. *Macromolecules* **1997**, *30*, 3832.
(32) TEMPO: 2,2,6,6-tetramethlylpiperidine-*N*-oxyl.
(33) Strobl, G. R. *Acta Crystallogr.* **1970**, *A26*, 367.
(34) Cameron, G. G. In *ESR Spectroscopy* in *Polymer Characterization*; Booth, C., Price, C., Eds.; London, 1987; Vol. 1, Chapter 23, p 517.
(35) Nishikawa, Y.; Kawada, H.; Hasegawa, H.; Hashimoto, T. *Acta Polym.* **1993**, *44*, 247.
(36) Hadziioannou, G.; Skoulios, A. *Macromolecules* **1982**, *15*, 258.
(37) Helfand, E.; Wassermann, Z. R. *Macromolecules* **1975**, *8*, 552.
(38) Hashimoto, T.; Shibayama, M.; Kawai, H. *Macromolecules* **1980**, *13*, 1237. Matsushita, Y.; Mori, K.; Saguchi, R.; Nakao, Y.; Noda, I.; Nagasawa, M. *Macromolecules* **1990**, *23*, 4313.
(39) Hashimoto, T.; Tsukahara, Y.; Kawai, H. *Macromolecules* **1981**, *14*, 708.
(40) Floudas, G.; Pakula, T.; Fischer, E. W. Hadjichristidis, N.; Pispas, S. *Acta Polym.* **1994**, *45*, 176.
(41) Stühn, B.; Mutter, R.; Albrecht, T. *Europhys. Lett.* **1992**, *18* (5), 427.
(42) Floudas, G.; Fytas, G.; Pispas, S.; Hadjichristidis, N.; Pakula, T.; Khokhlov, A. R. *Macromolecules* **1995**, *28*, 5109.
(43) Tsagaropoulos, G.; Kim, J.-S.; Eisenberg, A. *Macromolecule*s **1996**, *29*, 2222.
(44) Freed, J. H. Theory of Slow Tumbling ESR Spectra for Nitroxides In *Spin Labeling*; Berliner, L. J., Ed.; Academic Press: London, 1976.
(45) Wertz, J. E.; Bolton, J. R. *Electron Spin Resonance*; London, 1986; pp 197—203.
(46) The asymmetry in the dynamical profile of block copolymers is a quite general characteristic; see, e.g.: Gronski, W.; Stöppelmann, G.; Blume, A. *Polym. Prepr. (Am. Chem. Soc., Div. Polym. Chem.)* **1988**, *29* (1), 46. Denault, J.; Morèse-Séguéla, B.; Séguéla, R.; Prud'homme, J. *Macromolecules* **1990**, *23*, 4658.
(47) Spontak, R. J.; Smith; S. D.; Satkowski; M. M.; Ashraf; A.; Zielinski; J. M. In *Polymer Solutions, Blends and Interfaces*; Elsevier Science Publ.: 1992; pp 65—88. Spontak, R. J.; Zielinski; J. M. *Macromolecules* **1992**, *25*, 653.
(48) Matsushita, Y.; Mogi, Y.; Mukai, H.; Watanabe, J.; Noda, I. *Polymer* **1994**, *35*, 246.
(49) Matsen, M. W. *J. Chem. Phys.* **1995**, *102/9*, 3884.
(50) Lescanec, R. L.; Hadjuk, D. A.; Kim, G. Y.; Gan, Y.; Yin, R.; Gruner, S. M.; Hogen-Esch, T. E.; Thomas, E. L. *Macromolecules* **1995**, *28*, 3485.
(51) Broze, G.; Jérôme, R.; Teyssié; P. *Macromolecules* **1981**, *14*, 224. Broze, G.; Jérôme, R.; Teyssié; P., Marco, C. *Macromolecules* **1983**, *16*, 1771.
(52) Milner, S. T. *Macromolecules* **1994**, *27*, 2333.
(53) Se, K.; Yamazaki, H.; Shibamoto, T.; Takano, A.; Fujimoto, T. *Macromolecules* **1997**, *30*, 1570.
(54) For high star functionalities an ordered bicontinuous structure was found in some cases: Alward, D. J.; Kinning, E. L.; Thomas; Fetters, L. J. *Macromolecules* **1986**, *19*, 215.
(55) Ijichi, Y.; Hashimoto, T.; Fetters, L. J. *Macromolecules* **1989**, *22*, 2817.
(56) Gehlsen, M. D.; Almdal, K.; Bates, F. S. *Macromolecules* **1992**, *25*, 939.
(57) Matsen, M. W.; Schick, M. *Macromolecules* **1994**, *27*, 6761.
(58) Cf. Nyrkova, I. A.; Khokhlov, A. R.; Doi, M. *Macromolecules* **1993**, *26*, 3601.
(59) Mendes, E.; Schädler, V.; Marquez, C. M.; Lindner, P.; Wiesner, U. *Europhys. Lett.* **1997**, *40*, 521.

MA971843M